Applied Catalysis B: Environmental 182 (2016) 161–171

Contents lists available at ScienceDirect

Applied Catalysis B: Environmental

journal homepage: www.elsevier.com/locate/apcatb

Electrochemical advanced oxidation processes for sanitary landfill leachate remediation: Evaluation of operational variables

Francisca C. Moreira[a,*], J. Soler[a], Amélia Fonseca[b], Isabel Saraiva[b], Rui A.R. Boaventura[a], Enric Brillas[c], Vítor J.P. Vilar[a,*]

[a] LSRE - Laboratory of Separation and Reaction Engineering - Associate Laboratory LSRE/LCM, Departamento de Engenharia Química, Faculdade de Engenharia, Universidade do Porto, Rua Dr. Roberto Frias, 4200-465 Porto, Portugal
[b] Efacec Engenharia e Sistemas, S.A. (Unidade de Negócio Ambiente), Rua Eng. Frederico Ulrich - Guardeiras, Apartado 3003, 4471-907 Moreira da Maia, Portugal
[c] Laboratori d'Electroquímica dels Materials i del Medi Ambient, Departament de Química Física, Facultat de Química, Universitat de Barcelona, Martí i Franquès 1-11, 08028 Barcelona, Spain

ARTICLE INFO

Article history:
Received 3 June 2015
Received in revised form 17 August 2015
Accepted 5 September 2015
Available online 10 September 2015

Keywords:
Sanitary landfill leachate
EAOPs
Wastewater treatment
Photoelectro-Fenton
Operational variables

ABSTRACT

The effect of various parameters on the performance of electrochemical advanced oxidation processes (EAOPs) like electro-Fenton (EF), photoelectro-Fenton (PEF) and solar PEF (SPEF) was assessed for the treatment of a sanitary landfill leachate previously subjected to biological and coagulation processes. The tested operational variables included: (i) anode material (boron-doped diamond (BDD) and Pt), (ii) initial total dissolved iron concentration (20–80 mg L^{-1}), (iii) pH (2.8–4.0), (iv) initial addition of 1:3 Fe(III)-to-oxalate molar ratio at various pH values (2.8–5.0), (v) temperature (15–40 °C) and (vi) radiation source (UVA, UVA-Vis and UVC lamps and natural sunlight). The BDD anode showed high superiority over the Pt one for EF, PEF with UVA light (PEF-UVA) and SPEF processes, thereby advising an important role of the physisorbed hydroxyl radicals (•OH) at the anode surface on landfill leachate oxidation even under the potent solar radiation. An initial total dissolved iron content of 60 mg L^{-1} was chosen as the best dose for the PEF-UVA process with the BDD anode (PEF-BDD-UVA). While PEF-BDD-UVA without external addition of oxalic acid yielded the best results at pH 2.8, the initial addition of 1:3 Fe(III)-to-oxalate molar ratio allowed operating at pH 3.5 with even higher efficiency and at pH 4.0 with only slightly lower efficiency. Effluent temperatures from 20 to 40 °C led to similar mineralization rates for the PEF-BDD-UVA technique. The use of UVA and UVC lamps and natural sunlight as radiation sources in PEF-BDD and SPEF-BDD systems led to similar mineralization profiles as a function of time. The UVA-Vis lamp induced lower effluent mineralization mainly for longer reaction times.

1. Introduction

In recent years, electrochemical advanced oxidation processes (EAOPs) have been receiving increasing attention for the treatment of synthetic and real wastewaters [1–5]. The simplest and most popular EAOP is anodic oxidation (AO), where organics can be oxidized by: (i) direct electron transfer at the anode surface, (ii) highly reactive hydroxyl radicals (•OH) weakly adsorbed at the anode (M) surface, denoted as M(•OH), generated from water oxidation according to Eq. (1) and (iii) mediators electrogenerated in the bulk solution such as active chlorine species, ozone, persulfates and H_2O_2 [6,7].

$$M + H_2O \rightarrow M(^{\bullet}OH) + H^+ + e^- \quad (1)$$

In the last decade, more effective EAOPs based on Fenton's reaction chemistry, i.e. reaction between H_2O_2 and Fe^{2+} to originate •OH in the bulk according to Eq. (2) [8], have gained special attention. Electro-Fenton (EF) is the most known and widely applied EAOP based on Fenton's reaction and by definition [9] comprises: (i) the in situ and continuous electrogeneration of H_2O_2 at a carbonaceous cathode from the two-electron reduction of injected O_2 via Eq. (3), (ii) the addition of Fe^{2+} catalyst to the solution and (iii) the Fe^{3+} cathodically reduction to Fe^{2+} by Eq. (4).

$$H_2O_2 + Fe^{2+} \rightarrow Fe^{3+} + {}^{\bullet}OH + OH^- \quad (2)$$

* Corresponding authors. Fax: +351 225081674.
E-mail addresses: francisca.moreira@fe.up.pt (F.C. Moreira), vilar@fe.up.pt (V.J.P. Vilar).

http://dx.doi.org/10.1016/j.apcatb.2015.09.014
0926-3373/

$$O_{2(g)} + 2H^+ + 2e^- \rightarrow H_2O_2 \quad (3)$$

$$Fe^{3+} + e^- \rightarrow Fe^{2+} \quad (4)$$

The application of carbon-PTFE air-diffusion electrodes [2,10] and carbon felts [11,12] as cathodes for H_2O_2 electrogeneration has been particularly under focus. The EF process should not be confused with other variations like peroxi-coagulation, Fered-Fenton and electrochemical peroxidation often called EF. The peroxi-coagulation counts on H_2O_2 electrogeneration at the cathode as EF but uses a sacrificial iron anode for Fe^{2+} electrogeneration; the Fered-Fenton process involves the addition of both H_2O_2 and Fe^{2+} to the solution in an undivided cell along with Fe^{2+} regeneration from Eq. (4); and the electrochemical peroxidation generally involves a sacrificial iron anode for Fe^{2+} electrogeneration, an inert cathode where H_2 is produced from H_2O reduction and the addition of H_2O_2 to the solution [9].

Besides EF, photoelectro-Fenton (PEF) and solar PEF (SPEF) processes have also been receiving rising interest as the presence of artificial light (UVA, UVA-Vis and UVC) and natural sunlight, respectively [9], may accelerate the pollutants degradation by the photoreduction of Fe(III)-hydroxy complexes, such as the most photoactive $FeOH^{2+}$ at pH near 3 via Eq. (5) [13], and the direct photolysis of complexes established between Fe(III) and some organics by the general Eq. (6) [14–16], producing more Fe^{2+} and $^{\bullet}OH$.

$$FeOH^{2+} + h\nu \rightarrow Fe^{2+} + {}^{\bullet}OH \quad (5)$$

$$Fe^{3+}(L)_n + h\nu \rightarrow Fe^{2+}(L)_{n-1} + L^{\bullet}_{ox} \quad (6)$$

The treatment of sanitary landfill leachates by EAOPs has been mainly confined to the application of AO as a single stage, using anode materials like boron-doped diamond (BDD) [17–21], PbO_2 [21–23], SnO_2 [21,22] and other [24,25]. Nevertheless, some studies refer to the application of EAOPs based on Fenton's reaction such as Fered-Fenton and electrochemical peroxidation, as a single stage or combined with biological treatment, erroneously called EF [26–29]. Recently, Moreira et al. [30] have assessed for the first time the technical feasibility of integrating EF, PEF and SPEF processes in a multistage strategy for sanitary landfill leachate remediation. This multistage strategy was based on the European Patent EP 2 784 031 developed by Vilar and co-workers in cooperation with Efacec Engenharia e Sistemas, S.A. company [31] and embraced the following steps: (i) first biological process to remove the biodegradable organic fraction, oxidize ammonium and reduce alkalinity, (ii) coagulation of the bio-treated leachate with $FeCl_3$ to precipitate humic acids, suspended solids and other species that are able to filter the radiation and induce the electrochemical cell clogging, followed by separation of the clarified effluent, (iii) oxidation of the clarified effluent by an EAOP to degrade the recalcitrant compounds and increase its biodegradability and (iv) second biological process to degrade the biodegradable compounds generated during the EAOP and remove the remaining nitrogen content. In the cited study, the relative oxidation ability of EAOPs increased in the order EF < PEF ≤ SPEF and, furthermore, a current density (j) of 200 mA cm^{-2} was found as the best useful for application.

Despite all the previous work made, there is a lack of knowledge on the best operational conditions for sanitary landfill leachate treatment by EF, PEF and SPEF. In this context, this paper presents an unprecedented study on the influence of various key variables on the performance of EF, PEF and SPEF for the remediation of a sanitary landfill leachate previously subjected to biological and coagulation processes. The effect of anode material (boron-doped diamond (BDD) and Pt) was assessed for EF with two distinct initial total dissolved iron concentrations ($[TDI]_0$), PEF with UVA artificial light (PEF-UVA) and SPEF methods. The influence of $[TDI]_0$ (20–80 mg L^{-1}), pH (2.8–4.0), addition of Fe(III)-oxalate complexes at various pH values (2.8–5.0) and temperature (15–40 °C) was evaluated for PEF-UVA with a BDD anode (PEF-BDD-UVA). Beyond that, the effect of radiation source (UVA, UVA-Vis and UVC artificial lights and natural sunlight) was verified for PEF/SPEF-BDD.

2. Experimental

2.1. Chemicals

Concentrated sulfuric acid and sodium hydroxide, employed for pH adjustment, were of analytical grade supplied by Pronalab and Merck, respectively. Iron(II) sulfate heptahydrate, used as catalyst in trials without oxalic acid addition, was of analytical grade purchased from Panreac. Iron(III) chloride hexahydrate, used as catalyst in trials with oxalic acid addition and also applied in actinometric experiments, was of analytical grade supplied by Merck. Oxalic acid dihydrate, used as ligand and also employed in actinometric experiments, was of analytical grade acquired from VWR-Prolabo. Hydrogen peroxide 30% (w/v), used in photo-Fenton (PF) trials and in actinometric experiments, was of analytical grade purchased from Fisher Scientific. All the other chemicals were either of HPLC or analytical grade supplied by VWR-Prolabo, Sigma–Aldrich, Panreac, Merck, Fisher Scientific and Pronalab. Ultrapure and pure water used for analyses were obtained by a Millipore® Direct-Q system (18.2 MΩ cm resistivity at 25 °C) and a reverse osmosis system (Panice), respectively.

2.2. Pre-treated sanitary landfill leachate

A raw landfill leachate was collected in March and April 2014 from a municipal solid waste sanitary landfill located nearby Porto, Portugal. It was previously subjected to two treatment stages according to Saraiva et al. [31]: (i) biological treatment to remove the biodegradable organic fraction, oxidize ammonium and reduce alkalinity and (ii) coagulation of the bio-treated leachate with $FeCl_3$ to precipitate humic acids and particles that are able to filter the radiation and provoke the electrochemical cell clogging, with further separation of the clarified effluent. Since after these treatments high amounts of nitrite still available, causing additional H_2O_2 consumption and a large pH decrease during EAOPs, a third aeration stage at pH 3.3 was introduced. The complete characterization of the landfill leachate along all the treatment stages can be accessed in Moreira et al. [30]. Table 1 displays the main characteristics of the pre-treated sanitary landfill leachate employed in the current study. It had: (i) moderate yellowish brown color associated to the presence of fulvic acids and absence/low contents of humic acids [32], (ii) acid pH (2.2–2.9), (iii) high fraction of recalcitrant organic compounds, (iv) high conductivity that minimizes the energy consumption for electrochemical cell operation and (v) low [TDI] of 11–21 mg L^{-1}.

2.3. Experimental system

Electrochemical experiments were performed in a 2.2 L lab-scale flow plant mainly composed of: (i) a 1.5 L cylindrical glass vessel thermostatically controlled and magnetically stirred, (ii) a photoreactor with 694 mL of irradiated volume, comprising two stainless steel reflectors, i.e. double compound parabolic collector (CPC), that allocate a borosilicate tube in their focus with a concentric inner quartz tube where a lamp can be placed, and (iii) an electrochemical filter-press MicroFlowCell reactor from ElectroCell (Tarm, Denmark), employing a BDD or a Pt electrode as anode and a carbon-PTFE air-diffusion electrode as cathode, all of an active area of 10 cm^2. Moreira et al. [2] have comprehensively described these components.

UVA, UVA-Vis and UVC lamps were utilized. The UVA lamp was a Philips fluorescent blacklight blue lamp, 6 W energy power, model

Table 1
Main physicochemical characteristics of the pre-treated landfill leachate and discharge limits for wastewater treatment plants (WWTPs) final effluents according to Portuguese legislation (Decree-Law no. 236/98) and European Directive no. 91/271/CEE.

Parameter (units)	Pre-treated landfill leachate	ELV[a] for Decree-Law no. 236/98 or Directive no. 91/271/CEE
Color	Moderate yellowish brown	–
Color (diluted 1:20)	d.[b]	n.d.[c] (diluted 1:20) or -
Odor	Very weak	–
Odor (diluted 1:20)	n.d.[c]	n.d. [c] (diluted 1:20) or -
pH	2.2–2.9	6.0–9.0 or -
Temperature (°C)	20	3 °C increase[d] or -
Conductivity (mS cm^{-1})	18.9–20.3	–
Alkalinity (mg $CaCO_3$ L^{-1})	<5[e]	–
Turbidity (NTU)	5–6	–
Total dissolved carbon—TDC (mg L^{-1})	337–403	–
Dissolved inorganic carbon—DIC (mg L^{-1})	0.0–2.6	–
Dissolved organic carbon—DOC (mg L^{-1})	337–430	–
Chemical oxygen demand—COD (mg O_2 L^{-1})	1030–1505	150 or 125
5-day biochemical oxygen demand—BOD_5 (mg O_2 L^{-1})	1–10	40 or 25
BOD_5/COD	0.001–0.007	–
Total dissolved iron—TDI (mg L^{-1})	11–21	2.0 or -
Total suspended solids—TSS (mg L^{-1})	140–230	60 or 35
Total volatile solids—VSS (mg L^{-1})	72–138	–
Total nitrogen (mg L^{-1})	1450–2050	15 or 10
Total dissolved nitrogen (mg L^{-1})	1138–1256	–
Total dissolved organic nitrogen (mg L^{-1})	46–64	–
Ammonium—N—NH_4^+ (mg L^{-1})	<0.04 [e]–9	7.8 or -
Nitrite—N—NO_2^- (mg L^{-1})	3–18	–
Nitrate—N—NO_3^- (mg L^{-1})	1035–1192	11 or -
Sulfate—SO_4^{2-} (mg L^{-1})	1749–1917	2000 or -
Sulfite—SO_3^{2-} (mg L^{-1})	3.0–4.9	1.0 or -
Chloride—Cl^- (mg L^{-1})	3046–3822	–
Total phosphorous (mg L^{-1})	0.7–1.9	10 or 1
Phosphate—PO_4^{3-} (mg L^{-1})	<0.02 [e]	–
Calcium—Ca^{2+} (mg L^{-1})	183–271	–
Magnesium—Mg^{2+} (mg L^{-1})	120–136	–
Potassium—K^+ (mg L^{-1})	1948–2402	–
Sodium—Na^+ (mg L^{-1})	3010–3672	–

[a] ELV—Emission limit value.
[b] detected.
[c] not detected.
[d] Comparatively to the receptor medium.
[e] Limit of detection value.

TL 6W/08; the UVA-Vis lamp corresponded to a Luxram® UVA-Vis lamp, 6 W energy power; and the UVC lamp was a Philips UVC low pressure mercury lamp, 6 W energy power, model TUV G6T5. The characteristics of the lamps are given in Fig. 1 and Table 2. In SPEF trials, the photoreactor was tilted 41° (local latitude), the top reflector was removed and the solar radiation intensity was measured by a global UV radiometer (Kipp & Zonen B.V., model CUV5) placed at the same angle, which provides the incident UV intensity in W_{UV} m^{-2} from 280 to 400 nm. Moreira et al. [2], [5] have determined the photonic fluxes reaching the PEF-UVA and SPEF systems, respectively. These values were used to calculate the accumulated UV energy ($Q_{UV,n}$, in kJ L^{-1}) inside the reactor in a time interval Δt per unit of effluent volume according to Eqs. (7) and (8), respectively [5]:

$$Q_{UV,n} = 0.65 \frac{t_n}{V_s \times 1000} \quad (7)$$

$$Q_{UV,n} = Q_{UV,n-1} + \left(0.0121 \overline{UV}_{G,n} + 0.216\right) \frac{\Delta t_n}{V_s \times 1000}; \quad \Delta t_n = t_n - t_{n-1} \quad (8)$$

where 0.65 is the photonic flux reaching the PEF-UVA system (in J s^{-1}), t_n is the time corresponding to the n sample (in s), V_s is the solution volume (in L), 1000 is a conversion factor (in J kJ^{-1}), $\overline{UV}_{G,n}$

Table 2
Characteristics of UVA, UVA-Vis and UVC lamps and natural sunlight.

Light source	Average UV intensity (280–400 nm)[a] (W_{UV} m^{-2})	Photonic flux (300–410 nm)[b] (J s^{-1})	Photonic flux (250–450 nm)[c] (J s^{-1})	Photonic flux (250–500 nm)[d] (J s^{-1})
UVA lamp	30	0.65 ± 0.04[e]	–	–
UVA-Vis lamp	0.3	0.08 ± 0.01	–	0.23 ± 0.02
UVC lamp	0	–	0.72 ± 0.01	–
Natural sunlight[f]	46	0.77[g]	–	–

[a] Measured by a global UV radiometer (Kipp & Zonen B.V., model CUV5).
[b] Determined by 2-NB concentration actinometry.
[c] Determined by H_2O_2 actinometry.
[d] Determined by ferrioxalate actinometry using $[Fe(C_2O_4)_3]^{3-}$ ion prepared in situ.
[e] Determined in Moreira et al. [2].
[f] Under the current SPEF-BDD process.
[g] Calculated according to Eq. (8).

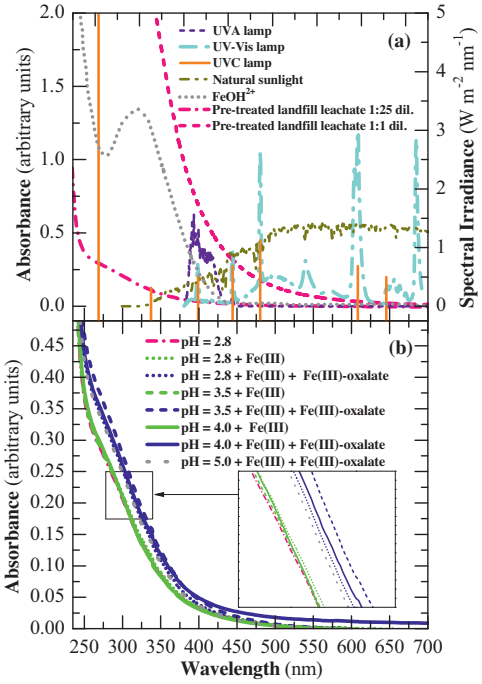

Fig. 1. (a) Spectral irradiance of UVA, UVA-Vis and UVC lamps and natural sunlight (UVA lamp: measured with the spectro-radiometer by Moreira et al. [2] and confirmed by Philips; UVA-Vis lamp: measured with the spectro-radiometer; UVC lamp: supplied by Philips; natural sunlight: AM1.5G reference spectrum [88]); absorption spectrum of $FeOH^{2+}$ at pH 2.9 [81]; absorption spectrum of the pre-treated sanitary landfill leachate at pH 2.8 (diluted 1:25 and without dilution). (b) Absorption spectra of the pre-treated sanitary landfill leachate at various pH values, with and without $[Fe^{3+}]$ = 60 mg L^{-1} and 1:3 Fe(III)-to-oxalate molar ratio (diluted 1:25).

is the average solar UV radiation (in W_{UV} m^{-2}) measured during the period Δt_n (in s) and ($0.0121\bar{U}V_{G,n}$ + 0.2161) is a correlation between the solar UV radiation (in W_{UV} m^{-2}) and the photonic flux (in J s^{-1}) valid for 18.5–50.0 W_{UV} m^{-2}.

2.4. Actinometric experiments

To determine the photonic flux in the PEF-UVA-Vis system, actinometry based on 2-nitrobenzaldehyde (2-NB) concentration and ferrioxalate actinometry using $[Fe(C_2O_4)_3]^{3-}$ ion prepared in situ were performed according to the procedure described in detail by Moreira et al. [2]. In turn, the photonic flux reaching the PEF-UVC system was assessed by the H_2O_2 actinometry described in Nicole et al. [33], which employed a 50 mM H_2O_2 solution prepared with pure water at pH 7.5. A volume of 1.250 L of this solution was added to the system and recirculated for 10 min in darkness, then the UVC lamp was switched on and samples were collected every 5 min for 60 min. The H_2O_2 concentration thus obtained was plotted as a function of irradiation time (s) and the curve was fitted to a zero-order kinetics. The photonic flux (F_0, in Einstein s^{-1}) was then calculated by Eq. (9):

$$F_0\left(\text{Einsteins}^{-1}\right) = \frac{d[H_2O_2]}{dt} \times \left(\frac{1}{\phi}\right) \times V \quad (9)$$

where $d[H_2O_2]/dt$ is the zero-order kinetics constant (mol L^{-1} s^{-1}), ϕ is the quantum yield of H_2O_2 at the lamp wavelength (1.11 at 205–280 nm for H_2O_2 [34]) and V is the solution volume (1.250 L).

Afterwards, the photonic flux was converted to J s^{-1} via Eq. (10):

$$F_0\left(\text{J s}^{-1}\right) = F_0\left(\text{Einsteins}^{-1}\right) \times E \times N_A \quad (10)$$

where E is the energy (J) calculated from Plank's equation for λ_{max} = 254 nm and N_A is Avogadro's number (6.022×10^{23} mol^{-1}).

2.5. Experimental procedure

The temperature controller was switched on at a temperature set-point that allowed to preserve the inner solution at 15, 20, 30 or 40 °C. A volume of 1.180 or 1.190 L of pre-treated landfill leachate was added to the glass vessel for trials without and with oxalic acid addition, respectively, and this effluent was homogenized by recirculation during 10 min in the dark (a 10 mL first control sample was taken). For trials without addition of oxalic acid, the pH was adjusted to 2.8–4.0 and the solution was homogenized for 10 min in the dark (a 10 mL second control sample was taken). Afterwards, $FeSO_4{\cdot}7H_2O$ was added (when applicable) to obtain a $[TDI]_0$ of 60 mg L^{-1}, taking into account the iron content of the effluent. Finally, the solution was homogenized for another 10 min in the dark (a 10 mL third control sample was taken). For trials with addition of Fe(III)-oxalate complexes, oxalic acid was added and the solution was homogenized for 10 min in the dark (a 10 mL second control sample was taken). Then, the pH was adjusted to 2.8–5.0 and the solution was subjected to homogenization for another 10 min in the dark (a 10 mL third control sample was taken). Lastly, $FeCl_3{\cdot}6H_2O$ was added to reach a $[TDI]_0$ of 60 mg L^{-1} and the solution was homogenized for other 10 min in the dark (a 10 mL fourth control sample was taken). A Fe(III)-to-oxalate molar ratio of 1:3 was used in these trials. j was set at 200 mA cm^{-2} and in light assisted EAOPs the radiation was simultaneously provided. Samples of 10 mL were taken at different time intervals to evaluate the degradation process. To remove impurities on the BDD and Pt surfaces and activate the cathode, the electrodes were previously polarized in a 7.0 g L^{-1} Na_2SO_4 solution at 100 mA cm^{-2} for 180 min.

2.6. Analytical determinations

Total dissolved carbon (TDC) and dissolved inorganic carbon (DIC) were measured in a Shimadzu TOC-V_{CSN} analyzer and the dissolved organic carbon (DOC) was calculated by the difference between TDC and DIC. Total dissolved nitrogen was determined in the same analyzer coupled with a TNM-1 unit. The specific energy consumption for electrochemical cell operation per unit DOC mass (EC_{DOC}, in kWh (kg DOC)$^{-1}$) and per unit volume (EC, in kWh m^{-3}) were calculated from Eqs. (11) and (12), respectively [35]:

$$EC_{DOC} = \frac{1000 E_{cell} I t}{V_s \Delta (DOC)_{exp}} \quad (11)$$

$$EC = \frac{E_{cell} I t}{V_s} \quad (12)$$

where 1000 is a conversion factor (in mg g^{-1}), E_{cell} is the average cell voltage (in V), I is the applied current (in A), t is the electrolysis time (in h), V_s is the solution volume (in L) and $\Delta(DOC)_{exp}$ is the experimental DOC concentration decay (in mg L^{-1}).

The solution pH and temperature were determined by a WTW inoLab 730 laboratory meter. Conductivity was measured by a HANNA Instruments HI 9828 Multiparameter meter. Alkalinity, turbidity, chemical oxygen demand (COD), 5-day biological oxygen demand (BOD_5), total suspended solids (TSS), volatile suspended solids (VSS), total nitrogen, total phosphorous and sulfite were measured according to the Standard Methods for the Examination of Water and Wastewater [36]. H_2O_2 content was assessed by the colorimetric metavanadate method [37]. TDI determination was based on the colorimetric 1,10-phenantroline standardized procedure [38]. UV–Vis measurements were carried out using a VWR UV-6300PC or a Merck Spectroquant® Pharo 100 spectrophotometer.

The UVA-Vis spectral irradiance was collected between 350 and 700 nm using a spectro-radiometer consisting of a mini spec-

trophotometer (USB2000 + UV–Vis, OceanOptics, USA) connected to an optical fiber (QP600-1-SR, OceanOptics, USA) with an irradiance probe on its tip (CC-3-UV-S cosine-corrected irradiance probe, OceanOptics,USA).

Inorganic anions were determined by ion chromatography by injecting 10 μL samples in a Dionex ICS-2100 LC equipped with an IonPac® AS11-HC, 250 mm × 4 mm, column at 30 °C and an anion self-regenerating suppressor (ASRS® 300, 4 mm) under isocratic elution of 30 mM NaOH at a flow rate of 1.5 mL min^{-1}. Inorganic cations were also assessed by ion chromatography but by injecting 25 μL samples in a Dionex DX-120 LC equipped with an IonPac® CS12A, 250 mm × 4 mm, column at ambient temperature and a cation self-regenerating (CSRS® Ultra II, 4 mm) suppressor under isocratic elution of 20 mM methanesulfonic acid at a flow rate of 1.0 mL min^{-1}.

Low-molecular-weight carboxylic acids (LMCA) were analyzed by ion-exclusion HPLC using a VWR Hitachi ELITE LaChrom fitted to a Phenomenex Rezex™ ROA-Organic Acid H+ (8%), 300 mm × 7.8 mm, column at ambient temperature (25 °C) and coupled to a diode array detector (DAD) set at λ = 210 nm. Samples of 10 μL were injected into the HPLC and the mobile phase was 0.0025 M H_2SO_4 at a flow rate of 0.5 mL min^{-1}. Before analysis, 1 M methanol, a well-known •OH scavenger ($k_{•OH} = 9.7 \times 10^8$ M^{-1} s^{-1}) [39], was added to samples to stop the mineralization process.

Before TDC, DIC, DOC, total dissolved nitrogen, TDI, inorganic ions and LMCA analysis, the samples were filtered with 0.45 μm Nylon filters from Whatman.

2.7. Model parameters estimation

A pseudo-first-order kinetic model was fitted to the DOC data as a simple mathematical model to quantitatively compare the DOC decay under various conditions. The kinetic model was adjusted by a nonlinear regression method using Fig.P software for Windows from Biosoft. The pseudo-first-order kinetic constant (k_{DOC}, in min^{-1}) was calculated from Eq. (13):

$$[DOC]_t = [DOC]_0 \times e^{-k_{DOC} \times t} \quad (13)$$

where $[DOC]_t$ and $[DOC]_0$ are DOC concentrations after t time and at time 0, respectively.

The fitting was performed by minimizing the sum of the squared deviations between experimental and predicted values. The goodness of fitting was assessed by calculating the relative standard deviations, the coefficient of determination (R^2) and the residual variance (S^2_R).

3. Results and discussion

3.1. Influence of anode material on EF, PEF-UVA and SPEF processes

BDD thin-film anodes are usually preferred for wastewater remediation as long as they exhibit a higher O_2-overpotential than classical anode materials such as Pt, RuO_2, IrO_2, PbO_2 and SnO_2, generating larger amounts of M(•OH) from Eq. (1) to react with organics [9,40]. Nevertheless, under SPEF conditions some waters contaminated with model pollutants have attained similar removals using both BDD and Pt anodes due to the improvement of contaminants removal by light-induced mechanisms, advising the use of Pt coated anode due to its lower price [2,41,42]. The effect of BDD and Pt anodes on the mineralization of a pre-treated landfill leachate was checked for EF with 12 mg $[TDI]_0$ L^{-1} (effluent content) and EF, PEF-UVA and SPEF with 60 mg $[TDI]_0$ L^{-1}, all at j of 200 mA cm^{-2}, pH 2.8 and 20 °C. These conditions were chosen because: (i) Saraiva et al. [31] have applied a $[TDI]_0$ of 60 mg L^{-1}, (ii) Moreira et al. [30] have determined that 200 mA cm^{-2} was the best j value for the pre-treated landfill leachate remediation by EAOPs, (iii) a pH of 2.8 is often assumed as optimal for Fenton-based processes [43,44] and (iv) 20 °C is an average leachate temperature commonly found in Portuguese sanitary landfill treatment plants [45].

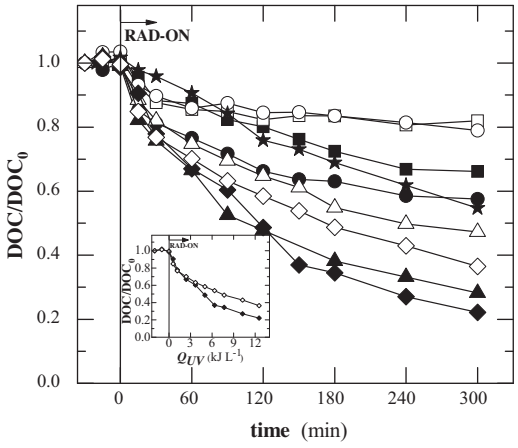

Fig. 2. Influence of anode material, (solid symbols) BDD and (open symbols) Pt, on normalized DOC removal as a function of time for degradations of the pre-treated landfill leachate under (■, □) EF with 12 mg $[TDI]_0$ L^{-1}, (●, ○) EF with 60 mg $[TDI]_0$ L^{-1}, (▲, △) PEF-UVA with 60 mg $[TDI]_0$ L^{-1} and (♦, ◊) SPEF with 60 mg $[TDI]_0$ L^{-1} processes at j = 200 mA cm^{-2}, pH = 2.8 and 20 °C. The inset panel depicts the normalized DOC removal in SPEF systems as a function of accumulated UV energy per L of solution. Extra process: (⋆) AO with 12 mg $[TDI]_0$ L^{-1} using BDD anode and Pt cathode at j = 200 mA cm^{-2}, pH = 2.8 and 20 °C.

Fig. 2 reveals higher DOC removals for all processes using BDD compared to the analogous methods using Pt, either in terms of time or accumulated UV energy per L of effluent (see the inset panel of Fig. 2). This suggests an important role of BDD(•OH) formed via Eq. (1) on the mineralization of the pre-treated landfill leachate even when light-induced reactions like Eqs. (5) and (6) enhance organics removal. These results contrast with the abovementioned achievements for waters spiked with model contaminants. Nonetheless, the superiority of BDD over Pt was slightly more emphasized in EF, with variances in the mineralization degree after 300 min of reaction of 1.9–2.0, 1.4 and 1.2 times for EF, PEF-UVA and SPEF, respectively.

Moreira et al. [30] have stated that the EAOP must provide a final landfill leachate with a DOC around 163 mg L^{-1} to fulfill the discharge limits into the environment after the further applied biological treatment. For the best EAOP, i.e. SPEF, energy consumptions for electrochemical cell operation of 137 or 277 kWh (kg DOC)$^{-1}$ (36 or 71 kWh m^{-3}) were required to reach this DOC value when applying BDD or Pt anode, respectively, with correspondent UV energy consumptions of 6.2 or 12 kJ L^{-1}, respectively. Considering an average electricity cost of 0.10 € kWh^{-1}, the electrochemical cell operation under SPEF conditions demanded the following electric energy costs to fulfill the discharge limits: around 14 € (kg DOC)$^{-1}$ and 3.6 € m^{-3} using the BDD anode and 28 € (kg DOC)$^{-1}$ and 7.1 € m^{-3} using the Pt anode. Note that the use of Pt anode led to a slightly lower cell voltage of 8.2 V compared to 8.5 V for BDD, but it was insufficient to promote lower energy consumptions due to the deeply lower mineralization ability of Pt(•OH).

Additionally, it was performed an assay under the same conditions as EF-BDD with 12 mg $[TDI]_0$ L^{-1} but using Pt as cathode in the absence of air supply to neglect the H_2O_2 electrogeneration, thereby establishing an AO-BDD process. Fig. 2 shows a slower DOC removal for AO-BDD in comparison to EF-BDD during the first 90 min of reaction, which can be related to the generation of •OH from Fenton's reaction Eq. (2) in the latter. Surprisingly, for longer times the mineralization was slightly faster for AO-BDD, which can

be explained by: (i) the loss of •OH from reaction with H_2O_2 via Eq. (14) [46] in EF-BDD and/or (ii) the generation of more recalcitrant by-products in EF-BDD.

$$H_2O_2 + {}^{\bullet}OH \rightarrow H_2O + HO_2^{\bullet} \quad (14)$$

3.2. Influence of initial total dissolved iron concentration on PEF-BDD-UVA process

The amount of TDI in solution is a crucial parameter for Fenton-based processes as it determines the Fenton's reaction Eq. (2) extent and thus the pollutants degradation. The best [TDI] in light-assisted Fenton-based EAOPs depends on various factors such as: (i) H_2O_2 concentration, (ii) system ability to regenerate Fe^{2+}, which can occur through photolysis of Fe(III)-hydroxy complexes by Eq. (5), photolysis of complexes between Fe(III) and organics via Eq. (6), cathodic reduction according to Eq. (4) and thermal Eqs. (15)–(17) [46,47], (iii) manifestation of inner filter effects, i.e. competitive absorption of photons between pollutants and Fe(III) photoactive species [46] and (iv) photoreactor geometry since the iron amount influences the light attenuation along the optical pathlength [46].

$$Fe^{3+} + H_2O_2 \rightarrow Fe^{2+} + HO_2^{\bullet} + H^+ \quad (15)$$

$$Fe^{3+} + HO_2^{\bullet} \rightarrow Fe^{2+} + O_2 + H^+ \quad (16)$$

$$Fe^{3+} + O_2^{\bullet -} \rightarrow Fe^{2+} + O_2 \quad (17)$$

Landfill leachate remediation by the conventional PF process has been applying iron contents in a wide range of 10–2000 mg L^{-1}, with highlighting on 60–80 mg L^{-1} [31,48–51]. Because of the cathodic Fe^{2+} regeneration through Eq. (4), the PEF and SPEF processes may allow to work at minor iron doses than in the chemical analogous processes.

$[TDI]_0$ of 20, 40, 60 and 80 mg L^{-1} were tested for the degradation of pre-treated landfill leachate by PEF-BDD-UVA at 200 mA cm^{-2}, pH 2.8 and 20 °C. Fig. 3a exhibits rising DOC abatements with the increment of iron content up to 60 mg $[TDI]_0$ L^{-1}, with similar DOC decays for 60 and 80 mg $[TDI]_0$ L^{-1}. Table 3 displays k_{DOC} values around 1.8 and 1.3 times superior for 60/80 mg $[TDI]_0$ L^{-1} when compared to 20 and 40 mg $[TDI]_0$ L^{-1}, respectively. These findings indicate that a $[TDI]_0$ of 60 mg L^{-1} ensured a maximum rate for Fenton's reaction Eq. (2), probably due to a maximum Fe^{2+} regeneration together with minimum inner filter effects and light attenuation along the current photoreactor optical pathlength. For all the trials, the DOC dropped more sharply in the first 15–30 min of reaction (13–29%) (see Fig. 3a) simultaneously with TDI decays of 8–18% (see Fig. 3b). This can be related to the precipitation of Fe(III) complexes with primary by-products probably formed through the attack of •OH provided by Fenton's reaction Eq. (2) since Moreira et al. [30] have attained a DOC decrease of around 20% together with a TDI decay of around 10% for a Fenton process using $[TDI]_0$ of 60 mg L^{-1}, $[H_2O_2]$ of 200–400 mg L^{-1}, pH 2.8 and 20 °C. Note that Fe^{3+} did not precipitate in the initial matrix of the pre-treated landfill leachate.

3.3. Influence of pH on PEF-BDD-UVA process and use of Fe(III)-oxalate complexes

Although the use of neutral pH in Fenton-based EAOPs could lead to acidification and neutralization prevention/minimization, it is well-known that higher pH values contribute to: (i) lower amounts of photoactive Fe(III)-hydroxy complexes in solution [16,43], (ii) iron precipitation [16,43], (iii) presence of carbonate and bicarbonate species, which reduce the process efficiency due to their •OH scavenging effect [39], (iv) reduction of the oxidation potential of •OH from 2.80 V at pH 0 to 1.95 V at pH 14 [52] and

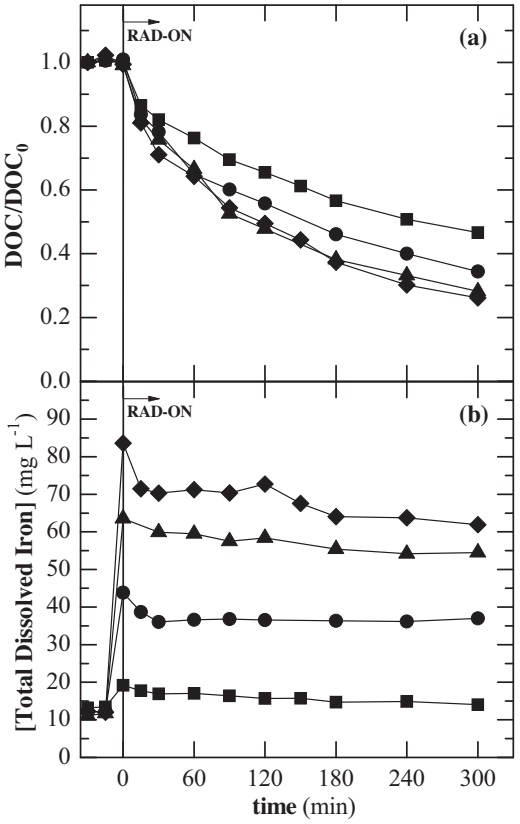

Fig. 3. Influence of initial total dissolved iron concentration ($[TDI]_0$) on (a) normalized DOC removal and (b) [TDI] as a function of time in PEF-BDD-UVA degradations of the pre-treated landfill leachate at j = 200 mA cm^{-2}, pH = 2.8 and 20 °C. $[TDI]_0$: (■) 20, (●) 40, (▲) 60 and (♦) 80 mg L^{-1}.

(v) rise of the auto-decomposition rate of H_2O_2 to water and oxygen, typically for pH above 5 [53]. In general, the application of conventional PF processes for the treatment of raw or pre-treated landfill leachate employ pH values between 2.5 and 3.5 as optimal [31,51,54–57]. Kim et al. [55] reported a decrease of 8% on the efficiency of a PF process for a raw landfill leachate remediation when operating at pH 4.0 in comparison to pH 3.0. Kim et al. [55] and Lau et al. [56] stated efficiency reductions of more than 30% for pH equal or above 5.0 when compared to pH ca.3.0 for a raw landfill leachate remediation by PF.

The influence of pH on the mineralization of the current pre-treated landfill leachate was tested at pH values of 2.8, 3.5 and 4.0 for a PEF-BDD-UVA process at 200 mA cm^{-2}, $[TDI]_0$ of 60 mg L^{-1} and 20 °C. Fig. 4a illustrates lower DOC decays for rising pH values and Table 3 reveals k_{DOC} values 2.0 and 2.7 times inferior for pH 3.5 and 4.0, respectively, in comparison to pH 2.8. The poorer mineralization at pH 3.5 and 4.0 came along with TDI precipitation from 60 to 16 and 10 mg L^{-1}, respectively, after 15–60 min of reaction, contrasting with the almost null iron precipitation achieved at pH 2.8 (see Fig. 4b). The theoretical Fe^{3+} speciation diagram shown in Fig. 5a outlines the presence of a maximum $FeOH^{2+}$ molar ratio at pH 2.8, the absence of this species for pH values above 3.4 and iron precipitation as $Fe(OH)_{3(s)}$ for pH values above 2.8, which agrees with the experimental results. Note that the possible formation of Fe(III)-carboxylate complexes generated from organics degradation was excluded in the speciation diagrams calculation since ion-exclusion HPLC analysis only detected formic acid in low contents below 14 mg C L^{-1}. The reduction in efficiency of 63% in terms of k_{DOC} attained in the current study from pH 3.0 to 4.0 contrasts with the drop in efficiency of 8% reached for the PF treatment of a raw landfill leachate in Kim et al. [55]. This is probably associated

Table 3
Pseudo-first-order kinetic constants for DOC removal (k_{DOC}) along with the corresponding coefficient of determination (R^2) and residual variance (S^2_R), obtained for the treatment of the pre-treated landfill leachate of Figs. 2–4, 6 and 7.

System		k_{DOC} ($\times 10^{-3}$ min^{-1})	R^2	S^2_R(mg^2 L^{-2})
Effect of BDD vs. Pt anode on various EAOPs	EF-12 mg [TDI]$_0$ L^{-1}-BDD	1.67 ± 0.04	0.993	19
	EF-12 mg [TDI]$_0$ L^{-1}-Pt	-[a]	-[a]	-[a]
	EF-60 mg [TDI]$_0$ L^{-1}-BDD	2.3 ± 0.1	0.994	12
	EF-60 mg [TDI]$_0$ L^{-1}-BDD	-[a]	-[a]	-[a]
	PEF-60 mg [TDI]$_0$ L^{-1}-BDD-UVA	4.3 ± 0.3	0.970	144
	PEF-60 mg [TDI]$_0$ L^{-1}-Pt-UVA	2.3 ± 0.1	0.986	45
	SPEF-60 mg [TDI]$_0$ L^{-1}-BDD	6.0 ± 0.2	0.991	129
	SPEF-60 mg [TDI]$_0$ L^{-1}-Pt	2.9 ± 0.1	0.997	17
		k_{DOC} (kJ L^{-1})	R^2	S^2_R(mg^2 L^{-2})
	SPEF-60 mg [TDI]$_0$ L^{-1}-BDD	0.14 ± 0.01	0.991	171
	SPEF-60 mg [TDI]$_0$ L^{-1}-Pt	0.069 ± 0.002	0.994	35
		k_{DOC} ($\times 10^{-3}$ min^{-1})	R^2	S^2_R(mg^2 L^{-2})
AO-12 mg [TDI]$_0$ L^{-1}-BDD		2.13 ± 0.04	0.995	18
Effect of initial total dissolved iron concentration (mg L^{-1}) on PEF-BDD-UVA	20	2.5 ± 0.1	0.995	14
	40	3.4 ± 0.1	0.993	37
	60	4.3 ± 0.3	0.970	144
	80	4.5 ± 0.2	0.991	62
Effect of pH on PEF-BDD-UVA	2.8	4.3 ± 0.3	0.970	144
	3.5	2.18 ± 0.04	0.996	3
	4.0	1.6 ± 0.1	0.986	14
Effect of 1:3 Fe(III)-to-oxalic molar ratio addition at various pH on PEF-BDD-UVA	2.8	5.8 ± 0.5	0.992	264
	3.5	9.5 ± 0.4	0.992	199
	4.0	4.4 ± 0.1	0.998	25
	5.0	1.7 ± 0.1	0.980	48
Effect of temperature (°C) on PEF-BDD-UVA	15	0.73 ± 0.03	0.981	9
	20	4.3 ± 0.3	0.970	144
	30	4.5 ± 0.2	0.987	48
	40	6.1 ± 0.2	0.988	59
Effect of temperature (°C) on PF-UVA	20	3.7 ± 0.1	0.991	53
	30	5.4 ± 0.2	0.986	67
	40	7.3 ± 0.3	0.988	111
Effect of light source on PEF-BDD and SPEF-BDD	UVA	4.3 ± 0.3	0.970	144
	UVA–Vis	3.6 ± 0.3	0.979	125
	UVC	4.0 ± 0.2	0.993	75
	Solar	6.0 ± 0.2	0.991	129
PEF-12 mg [TDI]$_0$ L^{-1}-BDD-UVC		3.47 ± 0.05	0.998	16

[a] No fitting of a pseudo-first-order kinetic model to experimental data.

to the overall lower efficiency of Kim et al. [55]'s AOP due to the precipitation of Fe(III) complexes with humic acids because their removal was not performed in a preliminary treatment.

The addition of carboxylic acids to Fenton-based processes can improve their efficiency because: (i) they promote the formation of more soluble complexes with Fe(III), allowing to maintain the iron in solution at higher pH values [58], (ii) Fe(III)-carboxylate complexes can absorb radiation in the UV–Vis range, being photodecarboxylated according to the general Eq. (6) with higher quantum yields for Fe^{2+} generation than that of Fe(III)-hydroxy complexes [14–16,59] and (iii) the establishment of Fe(III)-carboxylate complexes can avoid the formation of Fe(III)-sulfate, Fe(III)-chloride and Fe(III)-pollutants complexes in view of their higher formation constants in comparison with that of these species [60,61]. In this context, PF and PEF processes assisted by Fe(III)-carboxylate complexes have been applied to synthetic and real wastewaters [62–66]. Among these species, Fe(III)-oxalate complexes have gained larger attention due to their high quantum yield for Fe^{2+} formation, with major application in a 1:3 Fe(III)-to-oxalate molar ratio [15,65,67,68].

The effect of an initial 1:3 Fe(III)-to-oxalate molar ratio in the PEF-BDD-UVA process was verified for pH 2.8, 3.5, 4.0 and 5.0 (see Fig. 4a). For all these systems, the theoretical calculations point to the presence of 98–100% of total Fe^{3+} content in the form of $Fe(ox)_2^-$ and $Fe(ox)_3^{3-}$ species, which are the most photoactive Fe(III)-oxalate complexes [16], and null/almost null iron precipitation as $Fe(OH)_{3(s)}$ at the beginning of the process (see Fig. 5b). At pH 2.8, an initial 1:3 Fe(III)-to-oxalate molar ratio only led to slightly superior DOC decay in relation to the classical PEF-BDD-UVA method at the same pH, with a k_{DOC} value only 1.3 times higher (see Table 3), and the iron precipitation was similar and almost null (see Fig. 4b). In contrast, at pH 3.5 and 4.0 much higher mineralization rates upon addition of oxalic acid were found, with k_{DOC} values 4.4 and 2.8 times higher than the analogous processes without acid addition (see Table 3), respectively. This can be related to the gradual instead of abrupt iron precipitation (see Fig. 4b) and the greater absorption of UVA light highlighted in the absorption spectra of Fig. 1b. The addition of oxalic acid at pH 3.5 and 4.0 led to even higher or only slightly lower efficiencies than that obtained at pH 2.8 in the absence of oxalic acid addition, respectively. At pH 5.0, the PEF-BDD-UVA with oxalic acid addition reached the lowest DOC decay due to iron precipitation to values below 20 mg L^{-1} from 60 min of reaction (see Fig. 4b). Note that oxalic acid highly contributed to DOC content (76 mg C L^{-1}) and Fe(III)-oxalate complexes were rapidly photodecarboxylated, in only some minutes.

3.4. Influence of temperature on PEF-BDD-UVA process

In general, the efficiency of Fenton-based processes increases for higher temperatures owing to a faster Fe^{2+} regeneration by the

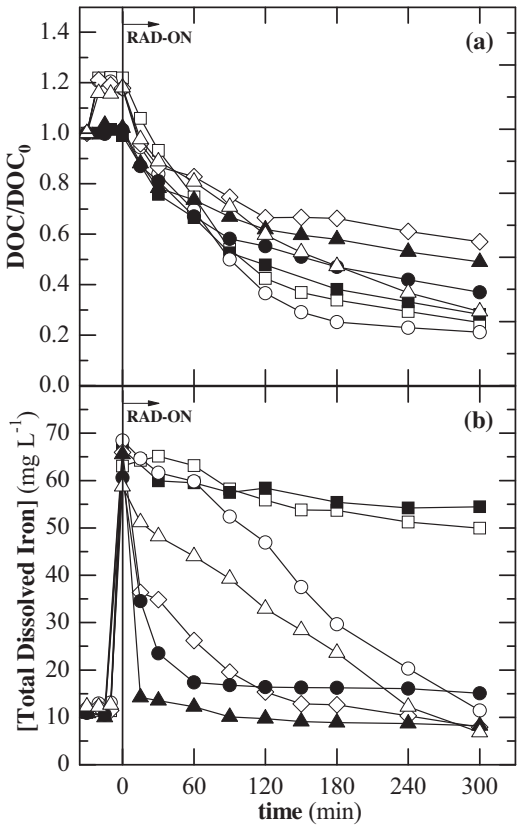

Fig. 4. Influence of pH and initial addition of 1:3 Fe(III)-to-oxalate molar ratio on (a) normalized DOC removal and (b) [TDI] as a function of time in PEF-BDD-UVA degradations of the pre-treated landfill leachate at $j = 200\,mA\,cm^{-2}$, $[TDI]_0 = 60\,mg\,L^{-1}$ and 20 °C. pH values for trials without oxalic acid addition: (■) 2.8, (●) 3.5 and (▲) 4.0. pH values for trials with oxalic acid addition: (□) 2.8, (○) 3.5, (△) 4.0 and (◊) 5.0.

thermal Eqs. (15)–(17) [46,47]. Moreover, the molar fraction of photoactive iron species and $Fe(OH)_{3(s)}$ can vary with temperature, as stated by Moreira et al. [65].

The influence of temperature on the mineralization of the pre-treated landfill leachate was assessed by applying temperatures of 15, 20, 30 and 40 °C in a PEF-BDD-UVA process at 200 mA cm^{-2}, $[TDI]_0$ of 60 mg L^{-1} and pH 2.8. Fig. 6a outlines quite similar DOC removals at 20, 30 and 40 °C together with a poorer mineralization at 15 °C, awarding a k_{DOC} value 5.9–8.4 times inferior (see Table 3). As can be seen in Fig. 6b, at 30 and 40 °C the TDI underwent decays of 31% and 68% after 300 min, respectively, whereas at 15 and 20 °C lower abatements below 18% were achieved. Taking into account all these results and the theoretical calculations on $FeOH^{2+}$ and $Fe(OH)_{3(s)}$ amounts given in Table 4, the following considerations can be carried out: (i) from 15 to 20 °C the increase on DOC removal can be attributed to higher rate of thermal Eqs. (15)–(17) and a slightly higher content of $FeOH^{2+}$, (ii) from 20 to 30 °C the theoretically predicted and experimentally observed iron precipitation as $Fe(OH)_{3(s)}$ might have compensate the increase of the rate of thermal Eqs. (15)–(17) and the slightly larger theoretical amount of $FeOH^{2+}$ and (iii) at 40 °C the highest iron precipitation along with the lower theoretical formation of $FeOH^{2+}$ when compared to 20 and 30 °C might diminish the positive effect of thermal Eqs. (15)–(17) rates. In addition, it is theoretically expected the increase on HSO_4^- content with rising temperature (see Table 4), which dictates increasing scavenging of •OH together with the formation of sulfate radical anions ($SO_4^{\bullet-}$) by Eq. (18) [69]. $SO_4^{\bullet-}$ are strong oxidants, being able to degrade organics, but they are weaker than •OH and they also lead to subsequent H_2O_2 decomposition via Eqs. (19) and (20) and Fe^{2+} oxidation according to Eq. (21) [69,70].

Table 4
Theoretical concentration of $FeOH^{2+}$, $Fe(OH)_{3(s)}$ and HSO_4^- at temperatures of 15, 20, 30 and 40 °C in a system containing the average amounts of NO_3^-, SO_4^{2-}, Cl^-, Ca^{2+}, Mg^{2+}, K^+ and Na^+ of the pre-treated landfill leachate (Table 1) and 60 mg Fe^{3+} L^{-1} (ionic strength of 0.390 M). Data were calculated by the chemical equilibrium modelling system MINEQL+ [89] using the equilibrium constants of Table SM-1 of Supplementary material.

	Species concentration at pH 2.8 (mg L^{-1})		
Temperature (°C)	$FeOH^{2+}$	$Fe(OH)_{3(s)}$	HSO_4^-
15	5.6	0	63
20	7.1	0	72
30	8.6	20	94
40	5.9	67	120

$$HSO_4^{\bullet-} + {}^{\bullet}OH \rightarrow SO_4^{\bullet-} + H_2O \quad (18)$$

$$SO_4^{\bullet-} + H_2O_2 \rightarrow SO_4^{2-} + H^+ + HO_2^{\bullet} \quad (19)$$

$$SO_4^{\bullet-} + HO_2^{\bullet} \rightarrow SO_4^{2-} + H^+ + O_2 \quad (20)$$

$$SO_4^{\bullet-} + Fe^{2+} \rightarrow Fe^{3+} + SO_4^{2-} \quad (21)$$

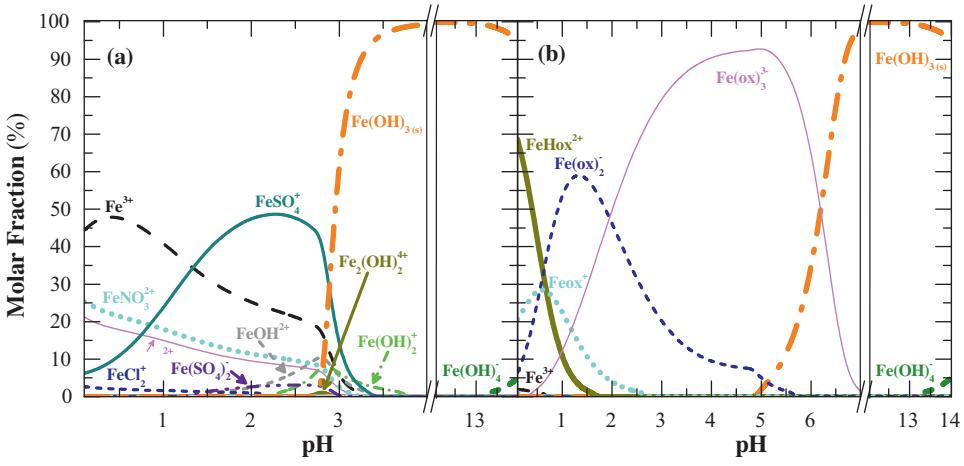

Fig. 5. Theoretical Fe^{3+} speciation diagrams as a function of the solution pH in the (a) absence and (b) presence of 1:3 Fe(III)-to-oxalate molar ratio for a system containing the average amounts of NO_3^-, SO_4^{2-}, Cl^-, Ca^{2+}, Mg^{2+}, K^+ and Na^+ of the landfill leachate after aeration (Table 1) and 60 mg Fe^{3+} L^{-1} (ionic strength of 0.390 M and 0.396 M, in the absence and presence of oxalic acid, respectively). Data were calculated by the chemical equilibrium modelling system MINEQL+ [89] using the equilibrium constants of Table SM-1 of Supplementary material. The formation of the solid iron phase $Fe(OH)_3$ was included in the calculation despite the slow formation of solid phases on the time scale of the experiments.

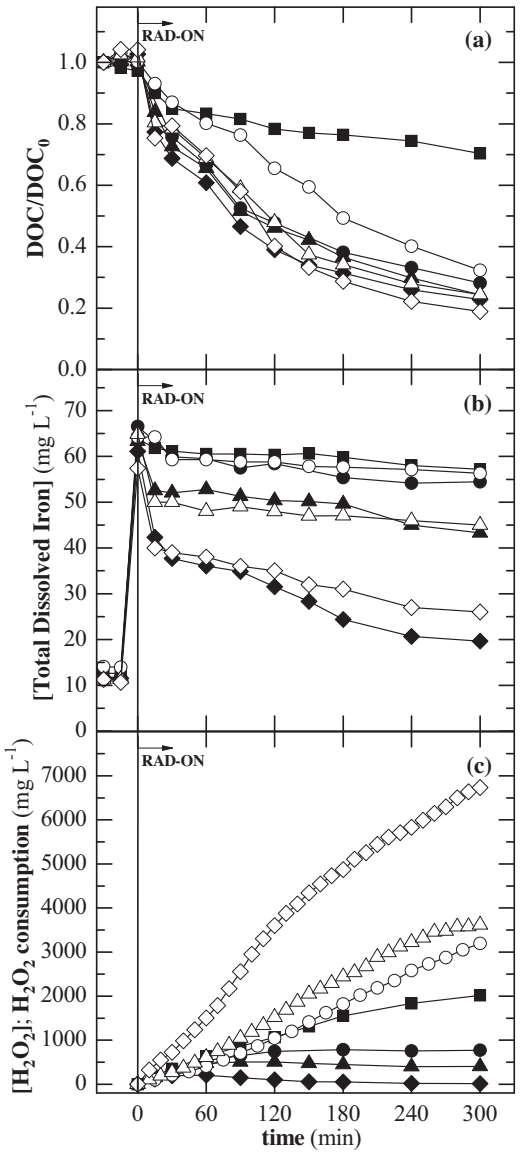

Fig. 6. Influence of temperature on (a) normalized DOC removal, (b) [TDI] and (c) H_2O_2 concentration (for PEF-BDD-UVA) or H_2O_2 consumption (for PF-UVA) as a function of time in (solid symbols) PEF-BDD-UVA and (open symbols) PF-UVA degradations of the pre-treated landfill leachate at $[TDI]_0$ = 60 mg L^{-1}, pH = 2.8, j = 200 mA cm^{-2} for PEF-BDD-UVA and $[H_2O_2]$ = 200–400 mg L^{-1} for PF. Temperature: (■) 15, (●, ○) 20, (▲, △) 30 and (♦, ◊) 40 °C.

Fig. 6c shows decreasing H_2O_2 accumulations with increasing temperature that can be related to the scavenging of this oxidant by Eqs. (15)–(17), (19) and (20). Note that the thermal decomposition of H_2O_2 into H_2O and O_2 may occur in large extent only for temperatures above 50 °C, being almost negligible in the temperature range tested [71].

In addition, conventional PF tests at 20, 30 and 40 °C were also performed using the same conditions as the PEF-BDD-UVA process but supplying H_2O_2 in multiple additions between 200 and 400 mg L^{-1} [72]. Besides the lower oxidation ability of PF-UVA comparatively to PEF-BDD-UVA at 20 °C already reported by Moreira et al. [30], Fig. 6a shows a high mineralization enhancement in PF-UVA from 20 to 30 °C, with a k_{DOC} value 1.5 times larger (see Table 3), contrasting with the almost null improvement attained for PEF-BDD-UVA. On the other hand, at 30 and 40 °C the mineralization ability of PF-UVA was quite similar, as occurred for PEF-BDD-UVA. These results suggest a larger participation of electrochemical reactions, i.e. BDD(•OH) generation from Eq. (1), cathodic Fe^{2+} regeneration via Eq. (4) and even the direct oxidation of organic compounds on BDD surface, on the effluent mineralization at 20 °C than at 30 and 40 °C, probably due to the increase of the rate of thermal Eqs. (15)–(17). Silva et al. [45] determined an increase in rate of more than 3 times from 21 to 37 °C for the PF treatment of a raw landfill leachate, higher than the enhancement achieved in this study, eventually mainly because of the composition of the effluent. Furthermore, Fig. 6b depicts quite alike iron decays for chemical and electrochemical processes and Fig. 6c shows a H_2O_2 consumption of more than double for PF at 40 °C compared to 20 and 30 °C due to the oxidant waste by Eqs. (15)–(17), (19) and (20).

3.5. Influence of radiation source on PEF-BDD and SPEF-BDD processes

Depending on the radiation source, different wavelengths will reach the solution, influencing: (i) the direct photolysis of pollutants, which takes place when the light source emits radiation at the same wavelength range as the contaminants can absorb radiation efficiently, (ii) the photoreduction of photoactive Fe(III)-hydroxy complexes and Fe(III) complexes with organics, especially those acting as ligands, that occurs under UV–Vis radiation according to Eqs. (5) and (6), respectively [16,73–76] and (iii) the generation of •OH in the presence of symmetrical peroxides such as H_2O_2 through the homolytic cleavage of the peroxide (—O—O—) bond that happens at 200–280 nm (UVC radiation) via Eq. (22) [77–79].

$$H_2O_2 + h\nu \rightarrow 2^{\bullet}OH \quad (22)$$

The most photoactive Fe(III)-hydroxy complex, i.e. $FeOH^{2+}$, has been reported to absorb radiation from 200 to 400 nm at pH 2.6–4.0 [73,80,81], following the behavior of Fig. 1a, with decreasing quantum yields for Eq. (5) from 280 to 370 nm (Φ = 0.29–0.08) [74]. In turn, photoactive Fe(III)-carboxylate complexes such as Fe(III)-oxalate, Fe(III)-citrate and Fe(III)-tartrate are able to absorb the visible light up to 500 nm with higher quantum yields for Fe^{2+} generation than $FeOH^{2+}$ [15,82].

Studies on PF for landfill leachate remediation have employed various light sources such as UVA lamps [55,56], natural sunlight [50,83] and UVC lamps [84] but no comparison between them has been performed. Regarding the PEF-BDD process, Moreira et al. [30] have only directly compared the efficiency between UVA artificial light and natural sunlight.

The effect of radiation source on the pre-treated landfill leachate treatment was assessed by employing UVA, UVA-Vis and UVC lamps and also natural solar radiation in PEF-BDD and SPEF-BDD processes at 200 mA cm^{-2}, $[TDI]_0$ of 60 mg L^{-1}, pH 2.8 and 20 °C. From Fig. 1a, one can conclude that both the artificial UVA-Vis light and the natural sunlight emit radiation in a 350–700 nm range, but while the UVA-Vis light exhibits various emission peaks, with emphasis for the larger peaks at 436, 546 and 611 nm, the solar radiation does not show severe fluctuations. In turn, the UVA lamp embraces a single and short UVA emission region from 350 to 410 nm, with λ_{max} = 360 nm, and the UVC lamp mainly emits at 254 nm, with very small emissions for higher wavelengths. Table 2 collects information on the characteristics of the light sources in terms of average UV intensity and photonic flux reaching the treated solution when they are employed. The solar radiation displayed a superior average UV intensity in the 280–400 nm range to that of the UVA lamp, with a 1.2 times greater photonic flux at 300–410 nm (2-NB actinometry), which would be even higher if the visible region was included. The UVA-Vis lamp at 250–500 nm (ferrioxalate actinometry) exhibited a photonic flux 2.8 and 3.3 times inferior to that of the UVA lamp and sunlight at 300–410 nm, respectively, and an almost null light emission from 300 to 410 nm,

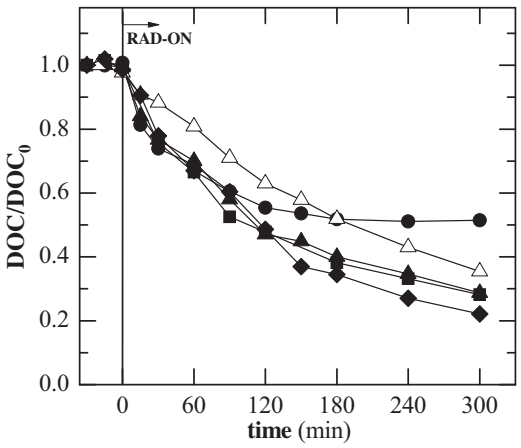

Fig. 7. Influence of radiation source on normalized DOC removal as a function of time in PEF-BDD and SPEF-BDD degradations of the pre-treated landfill leachate at $j = 200\ mA\ cm^{-2}$, $[TDI]_0 = 60\ mg\ L^{-1}$, pH = 2.8 and 20 °C. Radiation: (■) UVA, (●) UVA-Vis and (▲) UVC artificial light and (♦) natural sunlight with $\overline{UV}_{G,n} = 46\ W_{UV}\ m^{-2}$. (△) PEF-BDD-UVC process with $[TDI]_0 = 12\ mg\ L^{-1}$ (effluent content), $j = 200\ mA\ cm^{-2}$, pH = 2.8 and 20 °C.

suggesting a chiefly irradiation in the visible region. In turn, the UVC system exhibited a very similar photonic flux at 250–450 nm (H_2O_2 actinometry) to that of the UVA lamp at 300-410 nm. As UVA, UVA-Vis and UVC lamps have similar power energy (6 W) and dimensions, the PEF-BDD degradations using these three light sources can be directly compared in terms of time.

Preliminary trials on 300 min of photolysis of the pre-treated landfill leachate upon UVA, UVA-Vis and UVC artificial radiation and natural sunlight with $\overline{UV}_{G,n}$ of 45 $W_{UV}\ m^{-2}$ depicted very low mineralization decays near 4–8% (data not shown). This suggests the presence of very recalcitrant compounds in the landfill leachate that are not easily photoreduced, despite the ability of this effluent to absorb light up to 700 nm (see Fig. 1a). The high effluent absorbance may yield inner filter effects during PEF, resulting in a loss of photons efficiency since the photolysis of pollutants usually has lower quantum yield [46].

Fig. 7 shows only a slightly higher mineralization for the SPEF-BDD process in terms of time compared to the PEF-BDD-UVA one, with a k_{DOC} value 1.4 times higher (see Table 3), notwithstanding the superior photonic flux of solar radiation and its ability to emit in the visible region. This suggests that the photonic flux in the PEF-BDD-UVA process was able to induce almost maximum photoreduction of $FeOH^{2+}$ and/or Fe(III) complexes with organics by Eqs. (5) and (6), respectively. For the PEF-BDD-UVA-Vis, Fig. 7 displays a similar and fast DOC abatement for times up to 90 min in comparison to all the other processes, followed by a poor mineralization up to the end of reaction. The sharply DOC decay of 21% attained during the first 15 min of reaction was accompanied by a TDI decay of 20% (data not shown) and so it can be related to the abovementioned precipitation of Fe(III) complexes with primary by-products generated mainly due to •OH formed from Fenton's reaction Eq. (2). For longer times up to 90 min, it is likely that direct and/or indirect photolysis of some by-products might occur. The indirect photolysis corresponds to the formation of reactive species like •OH, peroxyl radicals (ROO•), singlet oxygen ($^1O_2$), carbon-centered radicals and excited triplet states from reactions involving the irradiation of, for example, fulvic acids [85–87]. For times above 90 min, the slow mineralization achieved suggests a small occurrence of $FeOH^{2+}$ photoreduction by UVA-Vis irradiation as expected in virtue of its poor light emission below 400 nm. Fig. 7 also exhibits similar DOC decays for the PEF-BDD-UVC and PEF-BDD-UVA treatments. Since the PEF-BDD-UVC process could count on the additional •OH production from the H_2O_2 photolysis according to Eq. (22), it is highly likely that the $FeOH^{2+}$ photoreduction occurred in lesser extent than for PEF-BDD-UVA, PEF-BDD-UVA-Vis and SPEF-BDD systems. An extra PEF-BDD-UVC process without iron addition, i.e. 12 mg $[TDI]_0\ L^{-1}$ (see Fig. 7 and Table 3), revealed a participation of 13% of the added 48 mg L^{-1} iron amount in the k_{DOC} value, which contrasts with the higher increment of 42% in k_{DOC} found for the PEF-BDD-UVA process when iron content rose from 20 to 60 mg L^{-1}, confirming the small role of $FeOH^{2+}$ photoreduction in PEF-BDD-UVC. Note that the H_2O_2 concentration was always higher than 300 mg L^{-1} for all the trials, thus ensuring the occurrence of Eqs. (2) and (22) (data not shown).

4. Conclusions

The mineralization of the pre-treated landfill leachate was faster for EF, PEF-UVA and SPEF processes with BDD anode when compared to the analogous processes using Pt anode, suggesting an important role of BDD(•OH) on the organics degradation even under the potent solar radiation. The use of a $[TDI]_0$ of 60 mg L^{-1} was chosen as the best dose for a PEF-BDD-UVA process, reaching similar effluent mineralization as 80 mg $[TDI]_0\ L^{-1}$. A pH of 2.8 yielded the highest pre-treated landfill leachate mineralization for a PEF-BDD-UVA process together with almost null iron precipitation. For higher pH values, iron precipitated progressively, thereby decreasing the mineralization rate. The initial addition of 1:3 Fe(III)-to-oxalate molar ratio to the system at pH 3.5 and 4.0 highly enhanced the DOC removal since it maintained iron dissolved in solution for longer reaction times, resulting in higher or only slightly lower efficiencies than at pH 2.8 in the absence of oxalic acid addition. The use of temperatures from 20 to 40 °C was affordable for the remediation of the pre-treated landfill leachate by PEF-BDD-UVA, presenting quite similar DOC decays, although temperatures above 20 °C led to iron precipitation. The application of UVA and UVC lamps and natural sunlight as radiation sources proved to be suitable for the current effluent remediation by PEF-BDD and SPEF-BDD since quite alike mineralization rates were achieved. The use of a UVA-Vis lamp led to lower effluent mineralization mainly for longer reaction times.

Acknowledgements

Financial support was partially provided by (i) AdvancedLFT project (reference FCOMP-01-0202-FEDER-033960), financed by FEDER (*Fundo Europeu de Desenvolvimento Regional*) under COMPETE program (*Programa Operacional Fatores de Competitividade*) of QREN (*Quadro de Referência Estratégico Nacional*) within the I&DT system (*Sistema de Incentivos à Investigação e Desenvolvimento Tecnológico*), (ii) UID/EQU/50020/2013 project, co-financed by FCT/MEC (*Fundação para a Ciência e a Tecnologia/Ministério da Educação e Ciência*) and FEDER under Program PT2020 and (iii) NORTE-07-0124-FEDER-0000008 project, co-financed by QREN, ON2 program (*Programa Operacional Regional do Norte*) and FEDER. F.C. Moreira acknowledges her Ph.D. fellowship SFRH/BD/80361/2011 supported by FCT. V.J.P. Vilar acknowledges the FCT Investigator 2013 Programme (IF/01501/2013).

Appendix A. Supplementary data

Supplementary data associated with this article can be found, in the online version, at http://dx.doi.org/10.1016/j.apcatb.2015.09.014.

References

[1] F.C. Moreira, S. Garcia-Segura, V.J.P. Vilar, R.A.R. Boaventura, E. Brillas, Appl. Catal. B Environ. 142–143 (2013) 877–890.

[2] F.C. Moreira, S. Garcia-Segura, R.A.R. Boaventura, E. Brillas, V.J.P. Vilar, Appl. Catal. B Environ. 160–161 (2014) 492–505.
[3] A.R.F. Pipi, A.R. De Andrade, E. Brillas, I. Sirés, Sep. Purif. Technol. 132 (2014) 674–683.
[4] E. Isarain-Chávez, C. De La Rosa, L.A. Godínez, E. Brillas, J.M. Peralta-Hernández, J. Electroanal. Chem. 713 (2014) 62–69.
[5] F.C. Moreira, R.A.R. Boaventura, E. Brillas, V.J.P. Vilar, Water Res. 75 (2015) 95–108.
[6] C.A. Martínez-Huitle, S. Ferro, Chem. Soc. Rev. 35 (2006) 1324–1340.
[7] M. Panizza, G. Cerisola, Chem. Rev. 109 (2009) 6541–6569.
[8] H.J.H. Fenton, J. Chem. Soc., Trans. 65 (1894) 899–910.
[9] E. Brillas, I. Sireís, M.A. Oturan, Chem. Rev. 109 (2009) 6570–6631.
[10] I. Sirés, E. Brillas, M. Oturan, M. Rodrigo, M. Panizza, Environ. Sci. Pollut. Res. 21 (2014) 8336–8367.
[11] M.A. Oturan, N. Oturan, M.C. Edelahi, F.I. Podvorica, K.E. Kacemi, Chem. Eng. J. 171 (2011) 127–135.
[12] A. El-Ghenymy, R.M. Rodríguez, E. Brillas, N. Oturan, M.A. Oturan, Environ. Sci. Pollut. Res. 21 (2014) 8368–8378.
[13] Y. Sun, J.J. Pignatello, Environ. Sci. Technol. 27 (1993) 304–310.
[14] O. Horváth, K.L. Stevenson, Charge Transfer Photochemistry of Coordination Compounds, VCH, New York, United States, 1992.
[15] Y. Zuo, J. Hoigne, Environ. Sci. Technol. 26 (1992) 1014–1022.
[16] B.C. Faust, R.G. Zepp, Environ. Sci. Technol. 27 (1993) 2517–2522.
[17] Á. Anglada, A. Urtiaga, I. Ortiz, D. Mantzavinos, E. Diamadopoulos, Water Res. 45 (2011) 828–838.
[18] A. Cabeza, A. Urtiaga, M.-J. Rivero, I. Ortiz, J. Hazard. Mater. 144 (2007) 715–719.
[19] A. Fernandes, M.J. Pacheco, L. Ciríaco, A. Lopes, J. Hazard. Mater. 199–200 (2012) 82–87.
[20] Á. Anglada, A.M. Urtiaga, I. Ortiz, J. Hazard. Mater. 181 (2010) 729–735.
[21] M. Panizza, C.A. Martinez-Huitle, Chemosphere 90 (2013) 1455–1460.
[22] A. Fernandes, D. Santos, M.J. Pacheco, L. Ciríaco, A. Lopes, Appl. Catal. B Environ. 148–149 (2014) 288–294.
[23] L.-C. Chiang, J.-E. Chang, T.-C. Wen, Water Res. 29 (1995) 671–678.
[24] N. Nageswara Rao, M. Rohit, G. Nitin, P.N. Parameswaran, J.K. Astik, Chemosphere 76 (2009) 1206–1212.
[25] H. Zhang, Y. Li, X. Wu, Y. Zhang, D. Zhang, Waste Manag. 30 (2010) 2096–2102.
[26] E. Atmaca, J. Hazard. Mater. 163 (2009) 109–114.
[27] S.H. Lin, C.C. Chang, Water Res. 34 (2000) 4243–4249.
[28] S. Mohajeri, H.A. Aziz, M.H. Isa, M.A. Zahed, M.N. Adlan, J. Hazard. Mater. 176 (2010) 749–758.
[29] D.-B. Zhang, X.-G. Wu, Y.-S. Wang, H. Zhang, Chem. Pap. 68 (2014) 782–787.
[30] F.C. Moreira, J. Soler, A. Fonseca, I. Saraiva, R.A.R. Boaventura, E. Brillas, V.J.P. Vilar, Water Res. 81 (2015) 375–387.
[31] I.M.A. Saraiva, M.A.F., Fonseca, V.J.P., Vilar, T.F.C.V., Silva, R.A.R. Boaventura, inventors. Efacec Engenharia e Sistemas, S.A., assignee. Method of treating leachate, phototreatment reactors and respective use. European Patent 2 784 031 2014 October 1.
[32] D.K. Nieder, Carbon and Nitrogen in the Terrestrial Environment, Springer Science + Business Media B.V., 2008, 2015.
[33] I. Nicole, J. De Laat, M. Dore, J.P. Duguet, C. Bonnel, Water Res. 24 (1990) 157–168.
[34] S. Goldstein, D. Aschengrau, Y. Diamant, J. Rabani, Environ. Sci. Technol. 41 (2007) 7486–7490.
[35] C. Flox, P.L. Cabot, F. Centellas, J.A. Garrido, R.M. Rodríguez, C. Arias, E. Brillas, Appl. Catal. B Environ. 75 (2007) 17–28.
[36] A.E. Clesceri, A.D. Greenberg, Standard methods for examination of water & wastewater, 21st ed., American Public Health Association (APHA), American Water Works Association (AWWA) & Water Environment Federation (WEF), 2005.
[37] R.F.P. Nogueira, M.C. Oliveira, W.C. Paterlini, Talanta 66 (2005) 86–91.
[38] ISO6332:1998, Water Quality- Determination of iron - Spectrometric Method Using 1,10-Phenanthroline, 1998.
[39] G.V. Buxton, C.L. Greenstock, W.P. Helman, A.B. Ross, J. Phys. Chem. Ref. Data 17 (1988) 513–886.
[40] A. Kapałka, G. Fóti, C. Comninellis, J. Appl. Electrochem. 38 (2008) 7–16.
[41] E. Guinea, C. Arias, P.L. Cabot, J.A. Garrido, R.M. Rodríguez, F. Centellas, E. Brillas, Water Res. 42 (2008) 499–511.
[42] M. Skoumal, R.M. Rodríguez, P.L. Cabot, F. Centellas, J.A. Garrido, C. Arias, E. Brillas, Electrochim. Acta 54 (2009) 2077–2085.
[43] J.J. Pignatello, Environ. Sci. Technol. 26 (1992) 944–951.
[44] A. Safarzadeh-Amiri, J.R. Bolton, S.R. Cater, Sol. Energy 56 (1996) 439–443.
[45] T.F.C.V. Silva, M.E.F. Silva, A.C. Cunha-Queda, A. Fonseca, I. Saraiva, R.A.R. Boaventura, V.J.P. Vilar, Chem. Eng. J. 228 (2013) 850–866.
[46] S. Malato, P. Fernández-Ibáñez, M.I. Maldonado, J. Blanco, W. Gernjak, Catal. Today 147 (2009) 1–59.
[47] A.Y. Sychev, V.G. Isak, Russ. Chem. Rev. 64 (1995) 1105–1129.
[48] J.L. de Morais, P.P. Zamora, J. Hazard. Mater. 123 (2005) 181–186.
[49] O. Primo, M.J. Rivero, I. Ortiz, J. Hazard. Mater. 153 (2008) 834–842.
[50] T.F.C.V. Silva, A. Fonseca, I. Saraiva, V.J.P. Vilar, R.A.R. Boaventura, Water Res. 47 (2013) 3543–3557.
[51] T.F.C.V. Silva, M.E.F. Silva, A.C. Cunha-Queda, A. Fonseca, I. Saraiva, M.A. Sousa, C. Gonçalves, M.F. Alpendurada, R.A.R. Boaventura, V.J.P. Vilar, Water Res. 47 (2013) 6167–6186.
[52] S.-M. Kim, A. Vogelpohl, Chem. Eng. Technol. 21 (1998) 187–191.
[53] R.E. Meeker, inventors. Stabilization of hydrogen peroxide. United States 3208825 A. 1965 September 28.
[54] D. Hermosilla, M. Cortijo, C.P. Huang, Sci. Total Environ. 407 (2009) 3473–3481.
[55] S.-M. Kim, S.-U. Geissen, A. Vogelpohl, Water Sci. Technol. 35 (1997) 239–248.
[56] I.W.C. Lau, P. Wang, S.S.T. Chiu, H.H.P. Fang, J. Environ. Sci. 14 (2002) 388–392.
[57] V.J.P. Vilar, E.M.R. Rocha, F.S. Mota, A. Fonseca, I. Saraiva, R.A.R. Boaventura, Water Res. 45 (2011) 2647–2658.
[58] Y. Sun, J.J. Pignatello, J. Agric. Food. Chem. 40 (1992) 322–327.
[59] A. Safarzadeh-Amiri, J.R. Bolton, S.R. Cater, Water Res. 31 (1997) 787–798.
[60] R.M. Smith, A.E. Martell, Sci. Total Environ. 64 (1987) 125–147.
[61] A.P.S. Batista, R.F.P. Nogueira, J. Photochem. Photobiol. A Chem. 232 (2012) 8–13.
[62] J.M. Monteagudo, A. Durán, J.M. Corral, A. Carnicer, J.M. Frades, M.A. Alonso, Chem. Eng. J. 181–182 (2012) 281–288.
[63] I.N. Dias, B.S. Souza, J.H.O.S. Pereira, F.C. Moreira, M. Dezotti, R.A.R. Boaventura, V.J.P. Vilar, Chem. Eng. J. 247 (2014) 302–313.
[64] D.R. Manenti, P.A. Soares, A.N. Módenes, F.R. Espinoza-Quiñones, R.A.R. Boaventura, R. Bergamasco, V.J.P. Vilar, Chem. Eng. J. 266 (2015) 203–212.
[65] F.C. Moreira, R.A.R. Boaventura, E. Brillas, V.J.P. Vilar, Appl. Catal. B Environ. 162 (2015) 34–44.
[66] P.A. Soares, M. Batalha, S.M.A.G.U. Souza, R.A.R. Boaventura, V.J.P. Vilar, J. Environ. Manag. 152 (2015) 120–131.
[67] Y.-H. Huang, S.-T. Tsai, Y.-F. Huang, C.-Y. Chen, J. Hazard. Mater. 140 (2007) 382–388.
[68] E.M. Rodríguez, B. Núñez, G. Fernández, F.J. Beltrán, Appl. Catal. B Environ. 89 (2009) 214–222.
[69] P. Neta, R.E. Huie, A.B. Ross, J. Phys. Chem. Ref. Data Reprints 17 (1988) 1027–1247.
[70] J. De Laat, G. Truong Le, B. Legube, Chemosphere 55 (2004) 715–723.
[71] A. Santos, P. Yustos, S. Rodriguez, E. Simon, F. Garcia-Ochoa, J. Hazard. Mater. 146 (2007) 595–601.
[72] J. Bacardit, I. Oller, M.I. Maldonado, E. Chamarro, S. Malato, S. Esplugas, J. Adv. Oxid. Technol. 10 (2007) 219–228.
[73] B.C. Faust, J. Hoigné, Atmos. Environ. A Gen. Top. 24 (1990) 79–89.
[74] H.-J. Benkelberg, P. Warneck, J. Phys. Chem. 99 (1995) 5214–5221.
[75] C. Weller, S. Horn, H. Herrmann, J. Photochem. Photobiol. A Chem. 268 (2013) 24–36.
[76] C. Weller, S. Horn, H. Herrmann, J. Photochem. Photobiol. A Chem. 255 (2013) 41–49.
[77] J.H. Baxendale, J.A. Wilson, Trans. Faraday Soc. 53 (1957) 344–356.
[78] W.H. Glaze, J.-W. Kang, D.H. Chapin, Ozone Sci. Eng. 9 (1987) 335–352.
[79] R. Venkatadri, R.W. Peters, Hazard. Waste Hazard. Mater. 10 (1993) 107–149.
[80] R.C. Turner, K.E. Miles, Can. J. Chem. 35 (1957) 1002–1009.
[81] V.A. Nadtochenko, J. Kiwi, Inorg. Chem. 37 (1998) 5233–5238.
[82] I.P. Pozdnyakov, A.V. Kolomeets, V.F. Plyusnin, A.A. Melnikov, V.O. Kompanets, S.V. Chekalin, N. Tkachenko, H. Lemmetyinen, Chem. Phys. Lett. 530 (2012) 45–48.
[83] C. Amor, E.D. Torres-Socías, J.A. Peres, M.I. Maldonado, I. Oller, S. Malato, M.S. Lucas, J. Hazard. Mater. 286 (2015) 261–268.
[84] A. Anfruns, J. Gabarró, R. González-Olmos, S. Puig, M.D. Balaguer, J. Colprim, J. Hazard. Mater. 258–259 (2013) 27–34.
[85] W.R. Haag, J. Hoigné, Environ. Sci. Technol. 20 (1986) 341–348.
[86] B.C. Faust, J. Hoigné, Environ. Sci. Technol. 21 (1987) 957–964.
[87] P.L. Brezonik, J. Fulkerson-Brekken, Environ. Sci. Technol. 32 (1998) 3004–3010.
[88] ASTM, Standard tables for reference solar spectral irradiances: direct normal and hemispherical on 37° tilted surface, 2003.
[89] D.C. Schecher, MINEQL+: a chemical equilibrium modeling system, in: Version 4.6 for Windows, Environmental Research Software, Hallowell, United States, 2007.